Energy scales in $4f^1$ delafossite magnets: Crystal-field splittings larger than the strength of spin-orbit coupling in $KCeO_2$

M. S. Eldeeb,[1] T. Petersen,[1] L. Hozoi,[1] V. Yushankhai,[2,3] and U. K. Rößler[1]
[1]*Institute for Theoretical Solid State Physics, Leibniz IFW Dresden, Helmholtzstrasse 20, 01069 Dresden, Germany*
[2]*Joint Institute for Nuclear Research, Joliot-Curie 6, 141980 Dubna, Russia*
[3]*Max-Planck-Institut für Physik komplexer Systeme, Nöthnitzerstrasse 38, 01187 Dresden, Germany*

(Received 4 September 2020; revised 29 October 2020; accepted 17 November 2020; published 4 December 2020)

Ytterbium-based delafossites with effective $\tilde{S} = 1/2$ moments are investigated intensively as candidates for quantum spin-liquid ground states. While the synthesis of related cerium compounds has also been reported, many important details concerning their crystal, electronic, and magnetic structures are unclear. Here we analyze the $\tilde{S}=1/2$ system $KCeO_2$, combining complementary theoretical methods. The lattice geometry was optimized and the band structure investigated using density functional theory extended to the level of a GGA+U calculation in order to reproduce the correct insulating behavior. The Ce $4f^1$ states were then analyzed in more detail with the help of *ab initio* wave-function-based computations. Unusually large effective crystal-field splittings of up to 320 meV are predicted, which puts $KCeO_2$ in the strong field coupling regime. Our results reveal a subtle interplay between ligand-cage electrostatics and the trigonal field generated by the extended crystalline surroundings, relevant in the context of recent studies on tuning the nature of the ground-state wave function in $4f$ triangular-lattice and pyrochlore compounds. It also makes $KCeO_2$ an interesting model system in relation to the effect of large crystal-field splittings on the anisotropy of intersite exchange in spin-orbit coupled quantum magnets.

DOI: 10.1103/PhysRevMaterials.4.124001

I. INTRODUCTION

Along with on-site Coulomb repulsion, spin-orbit coupling is considered to define a dominant energy scale in f-electron compounds. In $4f^{13}$ ytterbium oxides and chalcogenides, for example, materials that are investigated intensively nowadays as candidates for spin-liquid ground states [1–8], the separation between the low-lying states of the split $J=7/2$ ground-state multiplet and those of the excited $J=5/2$ term is in the range of 1.3 eV. Comparatively, the splittings induced by the ionic solid-state surroundings imply a scale of tens of meV [3–9]. A notable feature, however, is that for lighter ligands in these systems, i.e., O instead of S or Se, the crystal-field splittings may increase up to ≈100 meV [5–7,9]. This can be qualitatively explained by having shorter M-O bonds, which leads to stronger ligand-field effects, and also by more subtle chemical aspects giving rise to stronger trigonal compression of the oxygen cage in the oxides. Starting from such observations on Yb-based compounds, in particular the triangular-lattice $NaYbL_2$ delafossites [3–9], the Ce-based analogs, e.g., $KCeO_2$ [10], look from an electronic-structure point of view somewhat more peculiar: the Ce $4f$ states are known to be more extended, i.e., they are likely more sensitive to the ligand environment; on the other hand, the spin-orbit coupling is significantly weaker for early rare-earth ions by factors of ∼5 for Ce^{3+} as compared to Yb^{3+} [11]. An interesting regime can then be realized where spin-orbit interactions and crystal-field splittings have similar magnitude. Situations of this kind were discussed in the context of strong deviations from the $j_{\rm eff} = 1/2$ picture in t_{2g}^5 $5d$ and $4d$ quantum magnets such as $CaIrO_3$ [12,13] and α-$RuCl_3$ under high pressure [14], where the trigonal splittings imply a larger energy scale as compared to the strength of the $5d/4d$-shell spin-orbit coupling; they modify the nature of the ground-state wave functions and therefore the relevant intersite exchange paths. Looking for related physics in the case of $4f$ materials, we address the on-site electronic structure of Ce ions in $KCeO_2$. Impetus is also provided by recently finding crystal-field splittings of up to 125 meV in the sister compound $KCeS_2$ [15].

II. LATTICE GEOMETRY AND ELECTRONIC STRUCTURE FROM DENSITY FUNCTIONAL THEORY

While the synthesis of $KCeO_2$ was already reported decades ago [10], a complete characterization of its crystal structure is still missing. We therefore start our discussion with an analysis of structural aspects in $KCeO_2$, for which we rely on density-functional calculations with periodic boundary conditions. $KCeO_2$ crystallizes in the $NaFeO_2$-type delafossite structure with a rhombohedral lattice (space group $R\bar{3}m$, no. 166). In a hexagonal setting K, Ce, and O have the Wyckoff positions $3a$ (0, 0, 0), $3b$ (0, 0, 1/2), and $6c$ (0, 0, z), respectively (see Fig. 1). The experimental room-temperature lattice constants are $a = 3.66$ and $c = 18.66$ Å [10]. The position of O in the cell, i.e., the z parameter, has not yet been established. Using the delafossite setting, we determined this parameter and also performed a complete lattice optimization. The full-potential local-orbital code FPLO (version 18) [16]

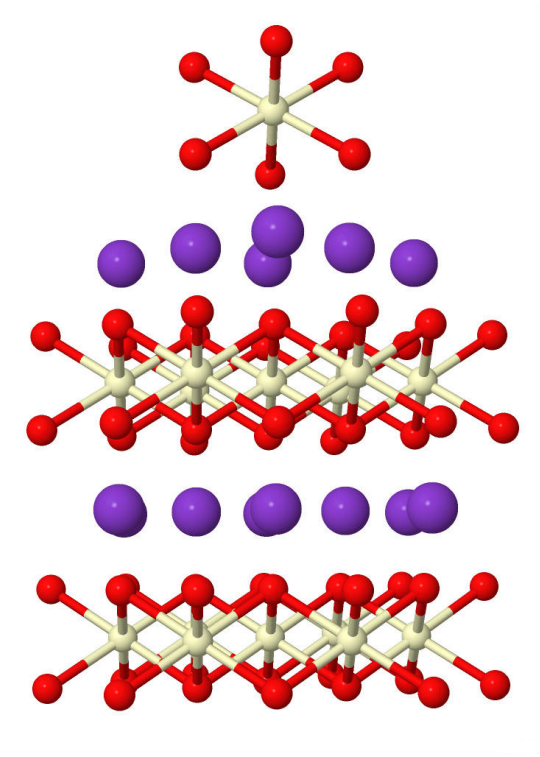

FIG. 1. Successive ionic layers in $KCeO_2$. Light yellow, red, and purple spheres represent Ce, O, and K sites, respectively. For the top CeO_2 layer, only one single CeO_6 octahedron is displayed.

was employed for this purpose. As an exchange-correlation functional we applied the generalized-gradient approximation (GGA) [17]. In the context of lattice optimization for $4f$ compounds, details on the performance of FPLO and of different functionals were recently published by Majumder *et al.* [18].

We first optimized the z parameter using the experimentally derived lattice constants and three different approaches: plain GGA with and without spin polarization, and also a GGA+U spin-split calculation. For the latter, the Coulomb repulsion parameter was set to $U = 5.0$ eV and the Hund exchange to $J_H = 0.69$ eV by fixing the Slater parameters for the $4f$ states of Ce to $F_0 = U$, $F_2 = 8.54$, $F_4 = 5.37$, and $F_6 = 3.86$ eV. The F_2 to F_6 ratio was adopted from Hartree-Fock calculations for free ions [19]; the value of J_H was renormalized by a factor of 0.7. The so-called atomic limit was used as double-counting correction. A k-mesh of $24 \times 24 \times 24$ points, corresponding to 13 824 irreducible k points, was found to be sufficiently accurate.

Results based on density functional theory (DFT) are listed in Table I. The data show that accounting for spin polarization has only a marginal influence on the lattice geometry, and also that the GGA+U scheme modifies the z parameter by only a small amount. Plain GGA yields a metallic state as Ce $4f$ bands show up at the Fermi level. On the other hand, in subsequent GGA+U calculations a finite gap arises. The densities of states for the three different approaches are compared in Fig. 2.

The optimization of the lattice parameters at the GGA+U level yields a too large lattice volume by about 3.5% as

TABLE I. Structural data obtained for $KCeO_2$ by various types of DFT computations. For the first four entries, the experimental lattice constants were used. Both scalar relativistic and fully relativistic calculations with spin-orbit coupling (SOC) were performed.

Method	a (Å)	c (Å)	z
GGA			0.2301
GGA spin-polarized	3.66[a]	18.66[a]	0.2304
GGA + U spin-polarized			0.2310
GGA + U + SOC			0.2311
GGA + U spin-polarized	3.694	18.964	0.2299
GGA + U + SOC	3.696	18.954	0.2299

[a]Fixed.

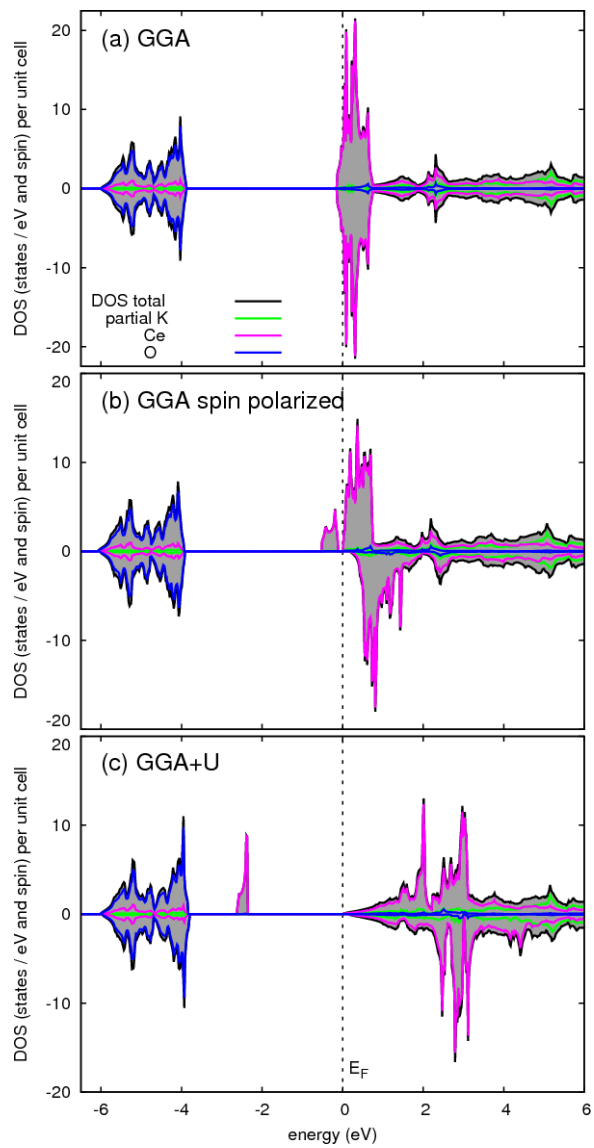

FIG. 2. Densities of states (DOSs) in $KCeO_2$ from DFT, including site-projected DOSs for the three different ionic species: results for spin-degenerate (a) and spin-polarized (b) plain GGA along with (c) GGA+U data. Spin-majority and -minority DOSs are plotted in the positive and negative ordinate direction, respectively, and the Fermi level E_F is at zero energy.

compared to experimental estimates [10]. This matches the usual tendency of the GGA functional to overestimate both volume and spin polarization. The cohesive energy of the compound is largely determined by the ionic contribution. The electronic states of Ce, in particular the $5d$'s, and their hybridization with O states do play a certain role, and an improved accuracy probably requires an improved description of electronic correlations. Yet, the relatively small effect on the O-ion position in the different DFT schemes suggests that the geometry optimization is reasonably robust and can be reliably used for a more detailed analysis of the Ce $4f$ electronic structure. The value computed by DFT for the O-ion z-axis fractional coordinate implies rather strong trigonal compression of the ligand cages, with O-Ce-O angles deviating by 7.7° from 90° bond angles. The impact of this trigonal distortion on the $4f$-shell energy level structure is discussed in the next section. For the quantum chemical calculations, we adopted the O z-axis parameter derived by GGA+U when using the experimental lattice constants.

III. QUANTUM CHEMICAL CALCULATIONS FOR THE Ce^{3+} $4f^1$ MULTIPLET STRUCTURE

In the intermediate-coupling regime with equally strong spin-orbit and crystal-field interactions, for describing the energy levels and the corresponding eigenstates of the $4f^1$ configuration of Ce^{3+}, the full basis of 14 atomiclike spin orbitals should be used. In addition to the value of the spin-orbit coupling λ, for D_{3d} point-group symmetry [10] six crystal-field parameters are required in the relevant effective model [20]. Fitting those effective interaction constants requires rather detailed experimental data—f-f excitation energies, g factors, etc. The situation becomes delicate when not all f-f transitions are captured in, e.g., the neutron scattering spectra [4] or additional peaks arise due to vacancies, interstitials, or strong electron-phonon couplings [15,21].

The associated uncertainties, however, can be overcome with the help of *ab initio* computations of the $4f$ multiplet structure. Using crystallographic data as on the third position in Table I, we performed such calculations for a finite set of atoms having a CeO_6 unit as a central region, in particular multiconfiguration and multireference quantum-chemical computations [22] both with and without spin-orbit coupling, and the main results are reported in Table II. An active space defined by the seven Ce $4f$ orbitals was employed to this end for the initial multiconfiguration calculation. The latter was carried out as a complete-active-space self-consistent-field (CASSCF) optimization [22] for an average of the seven $4f^1$ $S=1/2$ states. Multireference configuration-interaction (MRCI) wave functions were subsequently built by additionally considering single and double excitations [23] out of the Ce $4f$ and O $2p$ orbitals of the "central" CeO_6 octahedron. Effective core potentials and valence basis sets as optimized in Refs. [24,25] were used for the central Ce ion, along with all-electron [$4s3p2d$] Douglas-Kroll basis sets for the adjacent ligands [26]. To model the charge distribution in the immediate vicinity, we relied on large-core pseudopotentials including the $4f$ electrons in the core as concerns the 6 Ce nearest neighbors [27,28] and on total-ion potentials as concerns the 12 adjacent K sites [29]. The remaining part of the extended crystalline surroundings was modeled as an effective electrostatic field [30]. To determine the symmetries of the spin-orbit states, we computed the g factors for each of those and additionally the dipole transition matrix elements for $4f \rightarrow 5d$ excitations. For instance, the $4f^1$ spin-orbit states of $\Gamma_4+\Gamma_5$ symmetry can be quickly identified as those that have z-component dipole matrix elements [where z (c) coincides with the trigonal axis] with only two of the $5d^1$ spin-orbit states [31]. Larger active orbital spaces including both shells, $4f$ and $5d$, were used for obtaining the dipole transition matrix elements. The g factors were obtained according to the procedure described in Ref. [32]; by symmetry, the g_{ab} components vanish for the $\Gamma_4+\Gamma_5$ spin-orbit states. The quantum chemical package MOLPRO [33] was employed for all wave-function-based computations.

TABLE II. Ce^{3+} $4f^1$ multiplet structure (relative energies in meV) using fractional coordinates as optimized by DFT (see the text), CASSCF and MRCI data without spin-orbit coupling along with spin-orbit MRCI results (MRCI+SOC). For the double group, notations as in Ref. [34] (e.g., Appendix I in [34]) are used. The ground-state g factors are $g_c = 0.31$ and $g_{ab} = 0.09$.

	CASSCF	MRCI	MRCI+SOC	
$^2A_{2u}$	0	0	0	Γ_6
^2E_u	91	96	121	$\Gamma_4+\Gamma_5$
	91	96	143	Γ_6
$^2A_{1u}$	132	131	252	Γ_6
$^2E'_u$	226	229	352	$\Gamma_4+\Gamma_5$
	226	229	395	Γ_6
$^2A'_{2u}$	314	318	469	Γ_6

In the absence of spin-orbit interactions, an octahedral ligand field with full cubic symmetry splits the f levels into three sets—a_{2u}, t_{2u}, and t_{1u}—the latter two being triply degenerate. The a_{2u} orbital has its lobes normal to the facets of the ligand octahedral cage, and therefore the lowest energy because the Coulomb repulsion with electronic charge at the ligand sites is minimized; the t_{1u} orbitals, on the other hand, point directly toward the ligands and are of highest energy [35]. Since the smallest energy scale is defined by the a_{2u}-t_{2u} splitting [36], the a_{2u} and t_{2u} contributions to the ground-state spin-orbit wave function do not differ by much for cubic octahedral environment of the Ce ion [37]. Lowering the $4f$-site symmetry to trigonal (D_{3d} symmetry in the delafossite structure), the threefold degeneracy of the t_{2u} and t_{1u} states is lifted to yield $a_{1u}+e_u$ and $a_{2u}+e_u$ sets, respectively. As concerns the low-lying crystal-field levels in $KCeO_2$, surprisingly large a_{2u}-e_u and a_{2u}-a_{1u} splittings of 96 and 131 meV are computed by MRCI (see Table II). This provides a ground-state spin-orbit wave function that has significantly stronger contribution, 65%, from the lowest $^2A_{2u}$ trigonal-field term and only ∼35% from ^2E_u and $^2A_{1u}$. Since in this way the in-plane a_{2u}-a_{2u} superexchange is enhanced, the result is relevant to the analysis of the effective magnetic couplings (see [38–41] for a recent discussion of superexchange paths in rare-earth oxides and chalcogenides).

Having such strong crystal-field effects also gives rise to large excitation energies for the low-lying spin-orbit states.

TABLE III. Ce^{3+} $4f^1$ multiplet structure (relative energies in meV) for an idealized cubic CeO_6 octahedron, obtained by appropriately shifting the six ligands along the z coordinate, away from the reference Ce site. The ground-state g factors are $g_c = 0.64$ and $g_{ab} = 0.10$.

	CASSCF	MRCI	MRCI+SOC	
$^2A_{2u}$	0	0	0	Γ_6
$^2A_{1u}$	37	38	117	Γ_6
^2E_u	122	125	138	$\Gamma_4+\Gamma_5$
	122	125	248	Γ_6
$^2E'_u$	212	215	363	Γ_6
	212	215	375	$\Gamma_4+\Gamma_5$
$^2A'_{2u}$	220	225	425	Γ_6

By MRCI+SOC calculations [42], we find that the second and third spin-orbit doublets (relative energies of 121 and 143 meV in Table II) are separated by roughly the same amount from the ground state and from the next excited Kramers doublets. For a free ion, these next excited states are part of the $^2F_{7/2}$ manifold. While degenerate in vacuum, the higher-lying eight spin-orbit states cover an energy window of more than 200 meV in $KCeO_2$. For completeness, we also performed a calculation for a free Ce^{3+} ion, using the same basis sets and quantum chemical program. The $^2F_{5/2}$-$^2F_{7/2}$ splitting is $\Delta_{SOC} = 250$ meV by spin-orbit CASSCF. It implies a spin-orbit coupling constant $\lambda = 2\Delta_{SOC}/7 = 71$ meV [43], smaller by ≈20 meV than the a_{2u}-e_u splitting and smaller by a factor of ≈4.4 than the a_{2u}-a'_{2u} splitting in Table II. This λ is actually weaker than the corresponding parameter of, e.g., Ru^{3+} $4d^5$ ions on the Kitaev honeycomb lattice of α-$RuCl_3$ [44,45].

To put our results in perspective, we note that the lowest two excitation energies (121 and 143 meV; see Table II) are larger by factors of $\gtrsim$4 than the values reported for the Ce $2p$ halide CeF_3 [46]. While this can be qualitatively understood on the basis of the larger ligand ionic charges in the oxide, the difference is nevertheless remarkable. Compared to the sulfide $KCeS_2$ [15], the lowest excitation energies are larger by factors of 2–3 in $KCeO_2$, matching the trend pointed out by Gerlinger and Schaack when replacing Cl ($3p$ valence-shell ligand) by F ($2p$ ligand) within the Ce-halide CeX_3 family [46].

Interesting as well is that even for an artificial geometry having the six ligands around the reference Ce site shifted along the z coordinate away from the Ce ion such that the CeO_6 octahedron is cubic, the second and third spin-orbit doublets are still separated from each other by approximately 20 meV (see Table III). Since for an isolated cubic octahedron the lowest excited f^1 state is a Γ_8 quartet (see, e.g., [35,37]), this splitting of ≈20 meV points to the important role of structural anisotropies beyond the ligand coordination shell, confirming results of earlier studies on either $4f$, $5d$, or $4d$ compounds [9,32,47,48]. The trigonal ligand-cage compression and anisotropies of the extended environment seem in fact to work in opposite directions as concerns the e_u-a_{1u} and e'_u-a'_{2u} splittings: for the cubic octahedron (results in Table III), the a_{1u} level is lower in energy as compared to the e_u states, rather close to the a_{2u} component, while a_{1u} is above e_u with trigonal squeezing of the O_6 unit (see Table II); a similar trend is seen for the a'_{2u} level, although the latter does not move below e'_u when the trigonal squeezing is undone. The consequence of a reversed sequence of the e_u and a_{1u} crystal-field levels is an inverted sequence of the lowest two spin-orbit excited states (see also the model-Hamiltonian analysis in Ref. [49]).

Such modulations of the crystal-field splittings, e_u-a_{1u} and a_{2u}-a_{1u}, through (small) ligand displacements are also of interest in the context of electron-lattice couplings, i.e., the interaction between the nonspherical $4f$ electronic cloud and optical phonons. Electron-lattice couplings are known to be strong in Ce compounds (see, e.g., the discussion in Ref. [46]). They were invoked in relation to peculiar features in the Raman spectra of the tysonite trifluoride CeF_3 [46], and more recently they have been discussed as a possible mechanism behind the occurrence of low-intensity peaks in inelastic neutron scattering experiments on Ce^{3+} pyrochlores [21].

A related aspect analyzed in Ce^{3+} $4f^1$ pyrochlores is tailoring the e_u-$a_{2u,1u}$ splittings for realizing a $\Gamma_4 + \Gamma_5$ on-site spin-orbit ground state, associated with novel multipolar degrees of freedom and new topological characteristics [50–53]. An *ab initio* study such as that performed here on the interplay of ligand-cage distortions and anisotropic effects involving surroundings beyond the ligand coordination shell is also of interest for pyrochlore $4f$ compounds since it would better define the conditions under which the $\Gamma_4 + \Gamma_5$ ground state can be obtained. Important structural details in pyrochlore Ce^{3+} systems are (i) having two additional ligands on the trigonal axis (the ligand cage is defined by eight O ions in pyrochlores), and (ii) having less pronounced ionic charge imbalance [54] between the two different types of cation species in the immediate neighborhood (formally 4+ transition-metal and 3+ Ce nearby sites in the pyrochlores versus 3+ Ce and 1+ alkali nearby cations in the delafossite structure). These structural features in principle destabilize the a_{2u} and a_{1u} orbitals with respect to the e_u components. A $\Gamma_4 + \Gamma_5$ ground state can then be easily envisaged in $4f^1$ pyrochlores, but it does not seem likely in layered triangular-lattice compounds [55].

We also note that the corrections brought by MRCI to CASSCF are tiny, much less than in the case of $4f^{13}$ delafossites [9]. This can be understood to a large extent on the basis of the small number of electrons within the f shell; it also indicates that O-to-Ce charge-transfer effects do not play an important role [37]. Good agreement is therefore expected with experimental data on the on-site f-f excitations, coming from either inelastic neutron scattering or Raman spectroscopy. In the context of the growing interest in the research area of $4f$ delafossite-structure quantum magnets, with an extensive literature already available on $\tilde{S} = 1/2$ $4f^{13}$ delafossites [3–8], our analysis provides useful *ab initio* benchmarks for the electronic structure of "complemental" $\tilde{S} = 1/2$ $4f^1$ compounds.

IV. CONCLUSIONS

In summary, we present an *ab initio* investigation of the Ce f-shell multiplet structure in the triangular-lattice

compound $KCeO_2$. Using atomic positions as obtained by DFT lattice optimization, remarkably large crystal-field splittings are subsequently computed by wave-function-based quantum chemical methods. A regime that appears unusual for f-electron materials is realized this way, in which the splittings among the $4f$ levels as a result of anisotropic surroundings, up to ≈320 meV, are larger than both the spin-orbit coupling constant, $\lambda \approx 70$ meV, and characteristic free-ion $^2F_{5/2}$-$^2F_{7/2}$ splitting, $\Delta_{SOC} = 250$ meV. It remains to be seen how such a setting affects intersite spin interactions, through calculations based on either effective superexchange models [38–41] or on *ab initio* methods [44,56–59]. Crystal-field splittings as large as the strength of the spin-orbit coupling are also realized under high pressure in, e.g., the $4d^5$ Kitaev honeycomb compound α-$RuCl_3$; by modifying the composition of the ground-state wave function and the dominant exchange paths, they favor Heisenberg antiferromagnetism in that case [14]. Such findings in $4d^5$ materials suggest that $KCeO_2$ is an interesting model system in the $4f^1$ category.

ACKNOWLEDGMENTS

We thank D. Inosov, P. Fulde, and M. Richter for stimulating discussions, U. Nitzsche for technical assistance, and the German Research Foundation (Grant No. HO-4427/3) for financial support.

[1] Y. Li, H. Liao, Z. Zhang, S. Li, F. Jin, L. Ling, L. Zhang, Y. Zou, L. Pi, Z. Yang, J. Wang, Z. Wu, and Q. Zhang, Sci. Rep. **5**, 16419 (2015).
[2] Y. Li, G. Chen, W. Tong, L. Pi, J. Liu, Z. Yang, X. Wang, and Q. Zhang, Phys. Rev. Lett. **115**, 167203 (2015).
[3] W. Liu, Z. Zhang, J. Ji, Y. Liu, J. Li, H. Lei, and Q. Zhang, Chin. Phys. Lett. **35**, 117501 (2018).
[4] M. Baenitz, P. Schlender, J. Sichelschmidt, Y. A. Onykiienko, Z. Zangeneh, K. M. Ranjith, R. Sarkar, L. Hozoi, H. C. Walker, J.-C. Orain, H. Yasuoka, J. van den Brink, H. H. Klauss, D. S. Inosov, and T. Doert, Phys. Rev. B **98**, 220409(R) (2018).
[5] K. M. Ranjith, D. Dmytriieva, S. Khim, J. Sichelschmidt, S. Luther, D. Ehlers, H. Yasuoka, J. Wosnitza, A. A. Tsirlin, H. Kühne, and M. Baenitz, Phys. Rev. B **99**, 180401(R) (2019).
[6] L. Ding, P. Manuel, S. Bachus, F. Grußler, P. Gegenwart, J. Singleton, R. D. Johnson, H. C. Walker, D. T. Adroja, A. D. Hillier, and A. A. Tsirlin, Phys. Rev. B **100**, 144432 (2019).
[7] M. Bordelon, E. Kenney, T. Hogan, L. Posthuma, M. Kavand, Y. Lyu, M. Sherwin, C. Brown, M. J. Graf, L. Balents, and S. D. Wilson, Nat. Phys. **15**, 1058 (2019).
[8] P.-L. Dai, G. Zhang, Y. Xie, C. Duan, Y. Gao, Z. Zhu, E. Feng, C.-L. Huang, H. Cao, A. Podlesnyak, G. E. Granroth, D. Voneshen, S. Wang, G. Tan, E. Morosan, X. Wang, L. Shu, G. Chen, Y. Guo, X. Lu, and P. Dai, arXiv:2004.06867.
[9] Z. Zangeneh, S. Avdoshenko, J. van den Brink, and L. Hozoi, Phys. Rev. B **100**, 174436 (2019).
[10] R. Clos, M. Devalette, C. Fouassier, and P. Hagenmuller, Mater. Res. Bull. **5**, 179 (1970).
[11] D. Aravena, M. Atanasov, and F. Neese, Inorg. Chem. **55**, 4457 (2016).
[12] N. A. Bogdanov, V. M. Katukuri, H. Stoll, J. van den Brink, and L. Hozoi, Phys. Rev. B **85**, 235147 (2012).
[13] M. Moretti Sala, S. Boseggia, D. F. McMorrow, and G. Monaco, Phys. Rev. Lett. **112**, 026403 (2014).
[14] G. Bastien, G. Garbarino, R. Yadav, F. J. Martinez-Casado, R. Beltrán-Rodríguez, Q. Stahl, M. Kusch, S. P. Limandri, R. Ray, P. Lampen-Kelley, D. G. Mandrus, S. E. Nagler, M. Roslova, A. Isaeva, T. Doert, L. Hozoi, A. U. B. Wolter, B. Büchner, J. Geck, and J. van den Brink, Phys. Rev. B **97**, 241108(R) (2018).
[15] G. Bastien, B. Rubrecht, E. Haeussler, P. Schlender, Z. Zangeneh, S. Avdoshenko, R. Sarkar, A. Alfonsov, S. Luther, Y. A. Onykiienko, H. C. Walker, H. Kühne, V. Grinenko, Z. Guguchia, V. Kataev, H.-H. Klauss, L. Hozoi, J. van den Brink, D. S. Inosov, B. Büchner, A. U. B. Wolter, and T. Doert, SciPost Phys. **9**, 041 (2020).
[16] K. Koepernik and H. Eschrig, Phys. Rev. B **59**, 1743 (1999).
[17] J. P. Perdew, K. Burke, and M. Ernzerhof, Phys. Rev. Lett. **77**, 3865 (1996).
[18] M. Majumder, G. Simutis, I. E. Collings, J.-C. Orain, T. Dey, Y. Li, P. Gegenwart, and A. A. Tsirlin, Phys. Rev. Research **2**, 023191 (2020).
[19] J. B. Mann, *Atomic Structure Calculations. I. Hartree-Fock Energy Results for the Elements Hydrogen to Lawrencium*, Tech. Rep. (Los Alamos Scientific Lab., Los Alamos, NM, 1967).
[20] B. G. Wybourne, *Spectroscopic Properties of Rare Earths* (Interscience, New York, 1965).
[21] J. Gaudet, E. M. Smith, J. Dudemaine, J. Beare, C. R. C. Buhariwalla, N. P. Butch, M. B. Stone, A. I. Kolesnikov, G. Xu, D. R. Yahne, K. A. Ross, C. A. Marjerrison, J. D. Garrett, G. M. Luke, A. D. Bianchi, and B. D. Gaulin, Phys. Rev. Lett. **122**, 187201 (2019).
[22] T. Helgaker, P. Jørgensen, and J. Olsen, *Molecular Electronic-Structure Theory* (Wiley, Chichester, 2000).
[23] P. J. Knowles and H.-J. Werner, Theor. Chim. Acta **84**, 95 (1992).
[24] M. Dolg, H. Stoll, and H. Preuss, J. Chem. Phys. **90**, 1730 (1989).
[25] X. Cao and M. Dolg, J. Mol. Struct. (Theochem) **581**, 139 (2002).
[26] W. A. de Jong, R. J. Harrison, and D. A. Dixon, J. Chem. Phys. **114**, 48 (2001).
[27] M. Dolg, H. Stoll, A. Savin, and H. Preuss, Theor. Chim. Acta **75**, 173 (1989).
[28] M. Dolg, H. Stoll, and H. Preuss, Theor. Chim. Acta **85**, 441 (1993).
[29] P. Fuentealba, H. Preuss, H. Stoll, and L. von Szentpaly, Chem. Phys. Lett. **89**, 418 (1982).
[30] M. Klintenberg, S. E. Derenzo, and M. J. Weber, Comput. Phys. Commun. **131**, 120 (2000).
[31] I. Kebaili and M. Dammak, J. Theor. Appl. Phys. **6**, 21 (2012).
[32] N. A. Bogdanov, V. M. Katukuri, J. Romhányi, V. Yushankhai, V. Kataev, B. Büchner, J. van den Brink, and L. Hozoi, Nat. Commun. **6**, 7306 (2015).
[33] H. J. Werner, P. J. Knowles, G. Knizia, F. R. Manby, and M. Schütz, Wiley Rev.: Comp. Mol. Sci. **2**, 242 (2012).
[34] S. Sugano, Y. Tanabe, and H. Kamimura, *Multiplets of Transition-Metal Ions in Crystals* (Academic, New York, 1970).
[35] J. S. Griffith and L. E. Orgel, J. Chem. Phys. **26**, 988 (1957).

[36] There are rather detailed studies providing estimates for the a_{2u}–t_{2u} splitting in Ce halides with O_h symmetry; see, e.g., Table 3 in Ref. [11] and Fig. S1 in Ref. [37]. It implies a scale of ∼30 meV according to *ab initio* data reported in Ref. [11].
[37] W. W. Lukens, N. M. Edelstein, N. Magnani, T. W. Hayton, S. Fortier, and L. A. Seaman, J. Am. Chem. Soc. **135**, 10742 (2013).
[38] V. S. Mironov, J. Phys.: Condens. Matter **8**, 10551 (1996).
[39] A. V. Palii, Mold. J. Phys. Sci. **2**, 291 (2003).
[40] J. G. Rau and M. J. P. Gingras, Phys. Rev. B **98**, 054408 (2018).
[41] Y. Motome, R. Sano, S. Jang, Y. Sugita, and Y. Kato, J. Phys.: Condens. Matter **32**, 404001 (2020).
[42] A. Berning, M. Schweizer, H.-J. Werner, P. J. Knowles, and P. Palmieri, Mol. Phys. **98**, 1823 (2000).
[43] Somewhat smaller than estimates for Ce halides [11].
[44] R. Yadav, N. A. Bogdanov, V. M. Katukuri, S. Nishimoto, J. van den Brink, and L. Hozoi, Sci. Rep. **6**, 37925 (2016).
[45] P. Warzanowski, N. Borgwardt, K. Hopfer, J. Attig, T. C. Koethe, P. Becker, V. Tsurkan, A. Loidl, M. Hermanns, P. H. M. van Loosdrecht, and M. Grüninger, Phys. Rev. Research **2**, 042007(R) (2020).
[46] H. Gerlinger and G. Schaack, Phys. Rev. B **33**, 7438 (1986).
[47] V. M. Katukuri, K. Roszeitis, V. Yushankhai, A. Mitrushchenkov, H. Stoll, M. van Veenendaal, P. Fulde, J. van den Brink, and L. Hozoi, Inorg. Chem. **53**, 4833 (2014).
[48] N. A. Bogdanov, R. Maurice, I. Rousochatzakis, J. van den Brink, and L. Hozoi, Phys. Rev. Lett. **110**, 127206 (2013).
[49] W. G. Perkins and G. A. Crosby, J. Chem. Phys. **42**, 407 (1965).
[50] Y.-P. Huang, G. Chen, and M. Hermele, Phys. Rev. Lett. **112**, 167203 (2014).
[51] Y.-D. Li and G. Chen, Phys. Rev. B **95**, 041106(R) (2017).
[52] D. S. Inosov, Nat. Phys. **16**, 507 (2020).
[53] R. Sibille, N. Gauthier, E. Lhotel, V. Porée, V. Pomjakushin, R. A. Ewings, T. G. Perring, J. Ollivier, A. Wildes, C. Ritter, T. C. Hansen, D. A. Keen, G. J. Nilsen, L. Keller, S. Petit, and T. Fennell, Nat. Phys. **16**, 546 (2020).
[54] This is a main aspect discussed in, e.g., Refs. [9,48].
[55] Y.-D. Li, X. Wang, and G. Chen, Phys. Rev. B **94**, 201114(R) (2016).
[56] V. M. Katukuri, S. Nishimoto, V. Yushankhai, A. Stoyanova, H. Kandpal, S. Choi, R. Coldea, I. Rousochatzakis, L. Hozoi, and J. van den Brink, New J. Phys. **16**, 013056 (2014).
[57] N. Iwahara and L. F. Chibotaru, Phys. Rev. B **91**, 174438 (2015).
[58] F. Gendron, J. Autschbach, J.-P. Malrieu, and H. Bolvin, Inorg. Chem. **58**, 581 (2019).
[59] P. P. Hallmen, H.-J. Werner, D. Kats, S. Lenz, G. Rauhut, H. Stoll, and J. van Slageren, Phys. Chem. Chem. Phys. **21**, 9769 (2019).